Letter

Terahertz chiral subwavelength cavities breaking time-reversal symmetry via ultrastrong light-matter interaction

Johan Andberger, Lorenzo Graziotto, Luca Sacchi, Mattias Beck, Giacomo Scalari, and Jérôme Faist
Institute of Quantum Electronics, ETH Zürich, Auguste-Piccard-Hof 1, 8093 Zürich, Switzerland

(Received 6 October 2023; revised 27 February 2024; accepted 4 March 2024; published 26 April 2024)

We demonstrate terahertz chiral subwavelength cavities that break time-reversal symmetry by coupling the degenerate linearly polarized modes of two orthogonal sets of nanoantenna arrays using the inter-Landau-level transition of a two-dimensional (2D) electron gas in a perpendicular magnetic field, realizing normalized light-matter coupling rates up to $\Omega_R/\omega_{\mathrm{cav}} = 0.78$ with a dispersion that is modified by the parasitic capacitive coupling between the orthogonal antennas. The deep subwavelength confinement of the nanoantennas means that the ultrastrong-coupling regime can be reached even with a small number of carriers compared to Fabry-Pérot cavities, making it viable to be used with a variety of 2D materials. The nondegenerate circularly polarized ground state was only obtained after carefully optimizing the optical design to minimize the parasitic coupling to linearly polarized light.

DOI: 10.1103/PhysRevB.109.L161302

Introduction. A new class of quantum materials possessing nonclassical properties has emerged along with the growing understanding of how quantum effects control the macroscopic properties of matter [1]. Topological states of quantum matter exhibiting nonlocal properties emerging from its microscopic degrees of freedom have become a rapidly growing field in this regard, starting with the discovery of the first topologically nontrivial state, the quantum Hall state [2]. The quantization of the Hall conductivity in a two-dimensional electron gas (2DEG) arises due to the Berry curvature induced by the magnetic field breaking time-reversal symmetry. Classical light in the form of optical Floquet drives has recently emerged as a way to engineer the topological properties of quantum matter, exemplified by the Floquet topological insulator [3,4]. Circularly polarized light in particular has shown special promise for Floquet-induced topological band structures due to its potential for also breaking time-reversal symmetry [5,6]. Floquet engineering, where nonequilibrium light-matter states are formed by means of an external optical drive, possesses similarities to cavity quantum electrodynamics, where hybrid light-matter states are created by means of cavity strong light-matter interactions [7–10]. The prediction of a modified ground state containing virtual light excitations and matter excitations in the ultrastrong light-matter coupling regime has raised the possibility of engineering nontrivial topologies using the quantum fluctuations of a cavity [11]. The development of chiral cavities supporting nondegenerate circularly polarized modes by breaking time-reversal symmetry is especially important in this context.

The time-reversal symmetry of a cavity can be broken by means of strong light-matter coupling to the inter-Landau-level transition of a high-mobility two-dimensional electron gas in a perpendicular magnetic field [12]. The cyclotron motion of the electrons due to the Lorentz force has an angular frequency which lies in the terahertz (THz) range and is given by $\omega_c = eB/m^*$, where e is the electron charge, B is the magnetic flux density, and m^* is the effective electron mass. At low temperatures it becomes quantized into a harmonic system of Landau levels separated in energy by $\hbar\omega_c$ and due to Pauli's exclusion principle and angular momentum conservation the magnetic-field-dependent inter-Landau-level transition consists of the two Landau levels closest to the Fermi surface E_F. It has a large in-plane collective dipole moment due to the large dipole moment of the electron cyclotron motion combined with the large degeneracy of the Landau levels, given by $|\vec{d}| \propto el_B\sqrt{N_e}$, with N_e being the total electron density and $l_B = \sqrt{\hbar/eB}$ the magnetic length [13]. Therefore the rate of light-matter interaction quantified by the vacuum Rabi frequency $\Omega_R \propto \vec{d} \cdot \vec{E}_{\mathrm{vac}}$ can easily exceed the threshold for the ultrastrong-coupling regime of $\Omega_R/\omega_{\mathrm{cav}} > 0.1$ if this transition is coupled to the electric field $\vec{E}_{\mathrm{vac}}$ of a THz cavity mode, resulting in a hybrid light-matter system of Landau polaritons [14]. Metamaterial-based THz cavities containing such hybrid states possess the useful property of being easily accessible both optically using THz time-domain spectroscopy and by electronic magnetotransport measurements. In particular, since electronic measurements feature an energy scale of $\sim k_B T$, which at cryogenic temperatures is orders of magnitude smaller than the energy scale of the cavity resonance, they offer the possibility for studying the modified ground state of the ultrastrong-coupling regime [15,16].

Fabry-Pérot cavities breaking time-reversal symmetry have been demonstrated by incorporating a quantum well containing a two-dimensional electron gas [17]. In such cavities the two independent degenerate linearly polarized orthogonal modes are coupled by the inter-Landau-level transition of the 2DEGs placed in the center. The combined system can be described in terms of a Hopfield model [18] consisting of two degenerate circularly polarized modes, one left-hand circularly polarized (LCP) and one right-hand circularly polarized (RCP), where only the mode corotating with the cyclotron resonance couples actively, whereas the other

 ©2024 American Physical Society

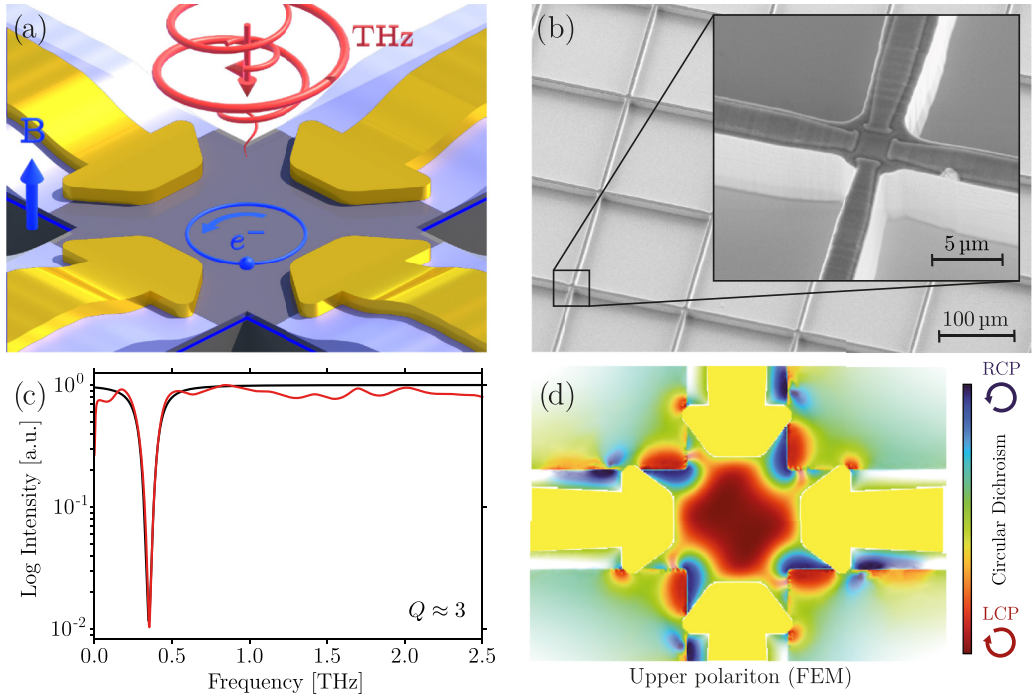

FIG. 1. (a) The linearly polarized nanoantenna modes are coupled to the time-reversal symmetry-breaking inter-Landau-level transition of the 2DEG (in blue), giving rise to nondegenerate circularly polarized modes. In a terahertz time-domain spectroscopy (THz-TDS) transmission measurement the cyclotron motion is either corotating or counter-rotating with the incoming circularly polarized THz pulse depending on the direction of the magnetic field, and therefore couples either to the lower and upper polariton modes or to the counter-rotating mode, respectively. (b) Scanning electron micrograph of a fabricated nanoantenna array (the inset shows a zoom-in on the unit cell). (c) Room-temperature THz-TDS transmission measurement at zero magnetic field (red curve) showing the presence of only a single well-pronounced cavity resonance together with the quality factor estimated using a Lorentzian fit (black curve). (d) Circular dichroism calculated from a finite-element simulation at the upper polariton frequency with $B = B_{\mathrm{cav}} = m^*\omega_{\mathrm{cav}}/e$ illustrating the chiral character of the mode in the region of the 2DEG. The image is weighted (using the alpha factor, i.e., the transparency) by the magnitude of the electric field to illustrate the degree of circular dichroism only where the field is the strongest.

counter-rotating mode is only coupled to the cyclotron resonance via the counter-rotating terms of the minimal coupling Hamiltonian. The resulting coupled system possesses three nondegenerate circularly polarized modes [19]: lower and upper polariton modes corotating with the electron cyclotron motion and a counter-rotating mode with a dispersion referred to as the vacuum Bloch-Siegert shift, after the first observed phenomenon in nuclear magnetic resonance under strong irradiation [20].

An advantage of using a metamaterial cavity instead of a Fabry-Pérot cavity is its deep subwavelength confinement, which leads to an extremely large electric field enhancement of a factor ∼100 and therefore a large vacuum electric field inside the cavity $E_{\mathrm{vac}} \sim 250\,\mathrm{V/m}$ due to the small effective mode volume $V_{\mathrm{eff}} \sim 10^{-9}(\lambda/2n)^3$. The ultrastrong-coupling regime is therefore reached with only ∼2000 electrons in the gap (see Supplemental Material A [21]). THz metamaterial cavities with a crosslike structure have previously been demonstrated [22], exhibiting both a deep subwavelength confinement and high-quality factor. However, the difficulty of obtaining two orthogonal linearly polarized modes coupled by a 2DEG in such geometries is challenging due to the significant capacitive coupling between the orthogonal directions. A half-wave dipole antenna consisting of two $\lambda/4$ dipole nanoantennas separated by a capacitor gap has a linearly polarized electric field inside the gap, and a cross-dipole or turnstile antenna consisting of two orthogonal half-wave dipole antennas with a mutual capacitor gap containing a 2DEG features the same electromagnetic components as the Fabry-Pérot cavity and is a conceptually simple way to implement a chiral subwavelength metamaterial cavity. The chiral cavity illustrated in Fig. 1(a) consists of an array of nanoantennas with length 150.5 μm, width 2.0 μm, and a mutual gap of 2.5 μm. A scanning electron micrograph of a fabricated array can be found in Fig. 1(b). An array was used in order to enhance the directionality of the antennas [23]. The resulting cross-dipole nanoantenna array in the absence of a magnetic field possesses a single resonance with frequency $f_{\mathrm{cav}} \approx 365\,\mathrm{GHz}$ and a quality factor $Q \approx 3$ determined from room-temperature THz time-domain spectroscopy measurements as shown in Fig. 1(c).

The antennas were defined and connected to a square mesa by a deep dry etching of 10 μm using a SiO_2 hard mask, which was chosen because of its relatively low THz refractive index of 2.1. Since the strength of the electric field in between the orthogonal antennas is proportional to the permittivity, this reduces the stray electric field and consequently also the amount of parasitic capacitive coupling. Patches were added to further reduce the parasitic interaction between the orthogonal nanoantennas and maximize the linear electric field inside

the capacitor gap that is coupled to the 2DEG. The degree of chirality of the design was quantified by the amount of *circular dichroism* [24],

$$\mathrm{CD} = \frac{|\vec{E}_{\mathrm{RCP}}|^2 - |\vec{E}_{\mathrm{LCP}}|^2}{|\vec{E}_{\mathrm{RCP}}|^2 + |\vec{E}_{\mathrm{LCP}}|^2}, \tag{1}$$

of the electric field in plane with the 2DEG with values ranging from perfectly LCP, -1, to perfectly RCP, $+1$. Figure 1(d) depicts the circular dichroism extracted from a finite-element simulation of the coupled system where the 2DEG was modeled as a gyrotropic material, i.e., with a tensorial conductivity. The in-plane electric field of the upper polariton mode was used to illustrate that in the antenna gap the electric field is mainly LCP. Regions with differing amounts of circular dichroism can be found outside of the antenna gap, showing also that the resulting cavity is not perfectly chiral. The cavity modes of nanoantennas differ from those of Fabry-Pérot cavities because the electric field is not strictly confined to the gap. The electric field from one half-wave dipole antenna will, due to the residual capacitive coupling and skin effect, modify the current distribution in the orthogonal one. This in turn changes the electric field distribution also inside the gap, making the electric fields of the two orthogonal modes not be fully linear and decoupled from each other.

Stripes of 2DEG were kept underneath the nanoantenna instead of etching patches of 2DEG in the capacitor gap as the latter would yield a two-dimensional (2D) plasma frequency proportional to $1/\sqrt{W}$, that with a width of $W = 2.5\,\mu\mathrm{m}$ would be $\omega_p/2\pi \sim 400\,\mathrm{GHz}$. This would lead to a zero-field value of the magnetoplasmon dispersion quasiresonant with the cavity and consequently a strong quenching of the coupling strength [25]. However, the presence of the 2DEG below the antenna arms gives rise to a continuum of magnetoplasmon modes [26]. The deep subwavelength confinement of the antennas means that the wavelength is much larger than the gap, which leads to diffraction. A large fraction of the light scattered from the gap will have a significant momentum component in plane with the 2DEGs and can be absorbed by this continuum. This leads to a reduction in transmission since these magnetoplasmon modes have large nonradiative losses due to their electric field being in plane with the 2DEGs. Because the frequency range of this continuum of modes is just above the cavity resonance, this leads to the disappearance of the signature of the upper polariton and counter-rotating modes at low magnetic fields, an effect referred to as polaritonic nonlocality [27]. To mitigate the impact of this effect the nanoantennas are lifted off the surface in the region outside the gap by a layer of SiO_2 with a thickness up to $1.0\,\mu\mathrm{m}$. A variation in the thickness of approximately 100 nm was introduced into this insulating SiO_2 layer by etching stripes at irregular distances and irregular widths before depositing the nanoantennas in order to further break up the continuum of magnetoplasmon modes [28].

High-mobility single and multiple quantum well GaAs/AlGaAs heterostructures were used for the fabrication of samples with different rates of light-matter interaction using standard clean-room photolithography techniques (see Supplemental Material D [21]). The fabricated samples were then measured using a THz time-domain spectroscopy setup with a bandwidth of 0.1–3 THz equipped with a split-coil superconducting magnet to probe the transmission as a function of perpendicular magnetic field from $B = -8\,\mathrm{T}$ to $B = +8\,\mathrm{T}$ [29]. Two broadband THz retarders mounted at an angle of 45° were used in order to measure the transmission of circularly polarized light. A vertically polarized terahertz pulse was generated using an interdigitated GaAs photoconductive antenna photoexcited by the femtosecond pulses from a 70-MHz Ti:sapphire laser, which was converted to circular polarization by the first THz retarder. The transmitted pulse after the sample was then converted back to vertical polarization by the second THz retarder for electro-optic detection, which was done using a 3-mm ⟨110⟩ *ZnTe* crystal. The incoming circularly polarized THz pulse is corotating with the electron cyclotron motion for $B < 0\,\mathrm{T}$ and therefore only couples to the corotating lower and upper polariton modes in this region whereas for $B > 0\,\mathrm{T}$ it couples to the counter-rotating mode. The cavities exhibit excellent agreement with the dispersion of a single-mode Hopfield model [13] when probed with linear polarization (see Fig. 7 in the Supplemental Material [21]) and the degree of chirality can therefore be determined by the degree of asymmetry between positive and negative magnetic fields and the agreement with the dispersion of the Hopfield model with circularly polarized modes (see Supplemental Material A [21] and Refs. [13,18,19] therein). Measurements of samples with a different number of quantum wells were used to study the system as a function of coupling strength (see Fig. 2).

Despite the measures taken the lower polariton and counter-rotating modes still exhibit significant broadening due to polaritonic nonlocality, which increases with the number of quantum wells. The upper polariton branch is also barely visible, as can be seen in Fig. 2. The lower polariton mode in the multiple quantum well samples also shows significant deviations from the Hopfield model, implying that despite the stripe geometry there is still the presence of a magnetoplasmon dispersion. A consequence of the mesa design is that the stripe geometry significantly modifies the Coulomb interaction configuration within the system. This can modify the dispersion of the magnetoplasmon modes and introduce a new category of low-frequency edge magnetoplasmon modes that are independent of the antenna [30]. Since these modes exist purely because of the stripe geometry they are not mitigated by lifting the antenna off the surface, and although they possess an acoustic dispersion and would consequently normally not be excited, because of the deep subwavelength confinement and subsequent diffraction they could induce significant absorption, and therefore also contribute to the disappearance of the polariton dispersion at low magnetic fields, in addition to modifying the dispersion of the lower polariton mode. To compensate for these effects the coupling strength was fitted only with the lower polariton mode at $B = -8\,\mathrm{T}$ and the counter-rotating mode at $B = +8\,\mathrm{T}$. The normalized coupling strengths $\Omega_R/\omega_{\mathrm{cav}}$ are however in excellent agreement with the expected $\sqrt{N_e}$ dependence of the total electron density, providing strong evidence for the chiral nature of the metamaterial.

The measurement of a single quantum well sample can be found in Fig. 3(a) together with the fitted normalized coupling strength. The dispersion shows excellent agreement for the LP mode, suggesting that in contrast to the

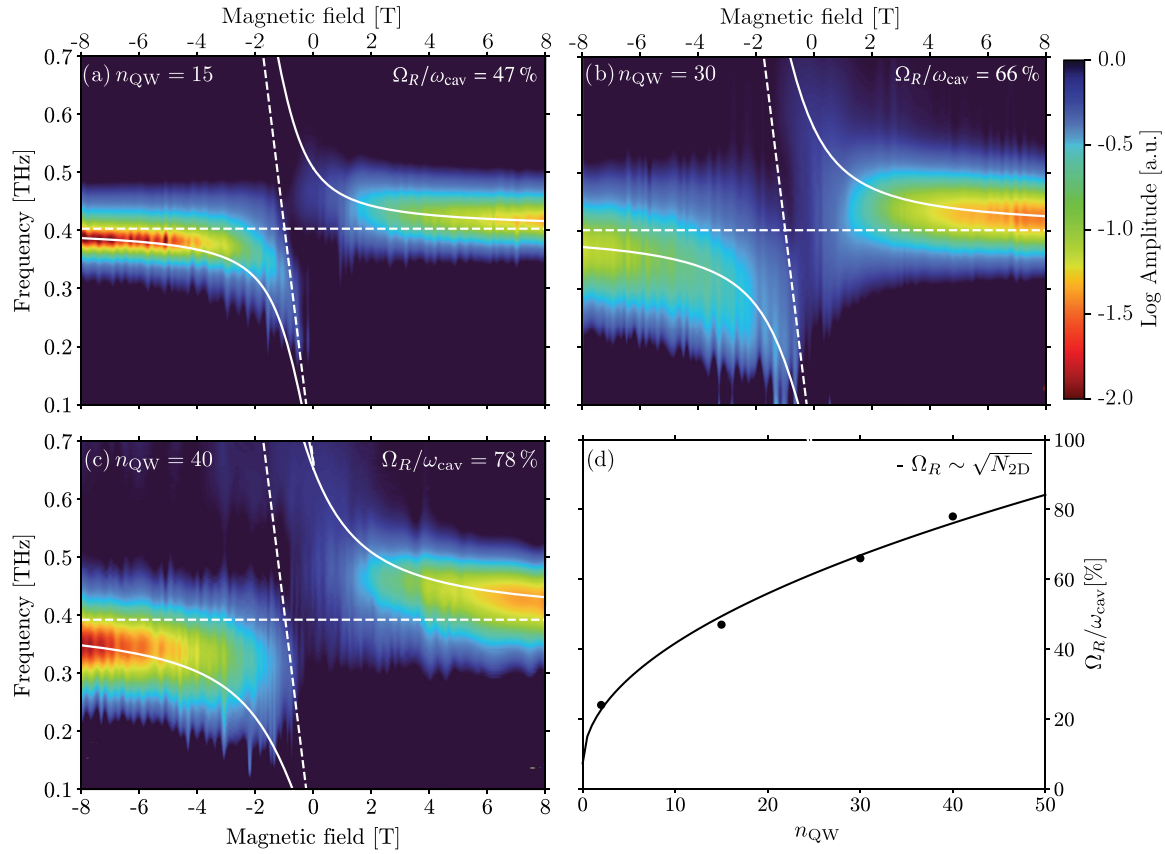

FIG. 2. Terahertz time-domain spectroscopy measurements of left-hand circularly polarized light as a function of perpendicular magnetic field at a temperature of $T = 3.2\,\mathrm{K}$ for samples with (a) 15 quantum wells, (b) 30 quantum wells, and (c) 40 quantum wells. (d) shows the scaling of the normalized coupling strength as a function of the number of quantum wells. The excellent agreement between the normalized light-matter coupling and its expected $\sqrt{N_e}$ dependence provides good evidence for the chirality of the nanoantenna arrays.

multiple quantum well samples there is no magnetoplasmon dispersion. The counter-rotating mode however is suppressed and deviates in the region of the cavity resonance. The vanishing of the counter-rotating and upper polariton modes at low magnetic fields can be understood in terms of the polaritonic nonlocality, which is still present despite the measures taken to mitigate it. To understand the deviation it should be noted that the deep subwavelength confinement of THz nanoantennas renders them suitable for modeling as lumped-element *RLC* circuits coupled by a gyrotropic material in the capacitor gap. It can be shown (see Supplemental Material B [21], including Refs. [31–34]) that a circuit model that takes the broken time-reversal symmetry into account possesses the same dispersion as the Hopfield model for a chiral Fabry-Pérot cavity, provided that there is negligible capacitive coupling between the nanoantennas outside the 2DEG region. In Fig. 3(b) the circuit transmission model in the absence of a parasitic interaction between the antennas is shown, together with the Hopfield dispersion. When a parasitic interaction is added, the counter-rotating mode at magnetic fields $B < B_{cav} \equiv m^*\omega_{cav}/e$ competes with the lower polariton mode due to the parasitic interaction in the case of a single quantum well, as can be seen in Fig. 3(c). The effects of the parasitic interaction include a modified dispersion and loss of the modes, an opening of a gap in the dispersion of the counter-rotating mode at $\omega_{cav} = \omega_c$, and magnetic field-dependent polarization states of the cavity modes. This model also explains why the effect of the parasitic interaction decreases with electron density and is therefore smaller in the multiple quantum well samples. Minimizing its effect requires minimizing the stray electric field outside the gap and maximizing the intracavity one. For such a field enhancement long nanoantennas were chosen to make the inductance as large as possible with respect to the capacitor gap for a given cavity frequency $\omega_{cav} \approx 1/\sqrt{L(C - C_{par})}$, where C_{par} denotes the parasitic capacitance between the orthogonal antennas.

Conclusion and outlook. We have demonstrated a THz chiral subwavelength cavity on the basis of including a time-reversal symmetry-breaking element, a 2DEG in a perpendicular magnetic field. The discrepancies between measurements and the circuit and Hopfield models can be understood within the framework of parasitic capacitive coupling between the orthogonal nanoantennas and polaritonic nonlocality due to their deep subwavelength confinement. The issue of polaritonic nonlocality remains significant despite the measures taken to mitigate it, with the measures only being effective in the single quantum well sample. This is most likely because the distance between the nanoantennas and the 2DEGs is still smaller than the total thickness of the multiple quantum well heterostructure, even for $n_{QW} = 15$. However, its effects of reducing transmission at low magnetic fields and vanishing of the upper polariton mode does not impact

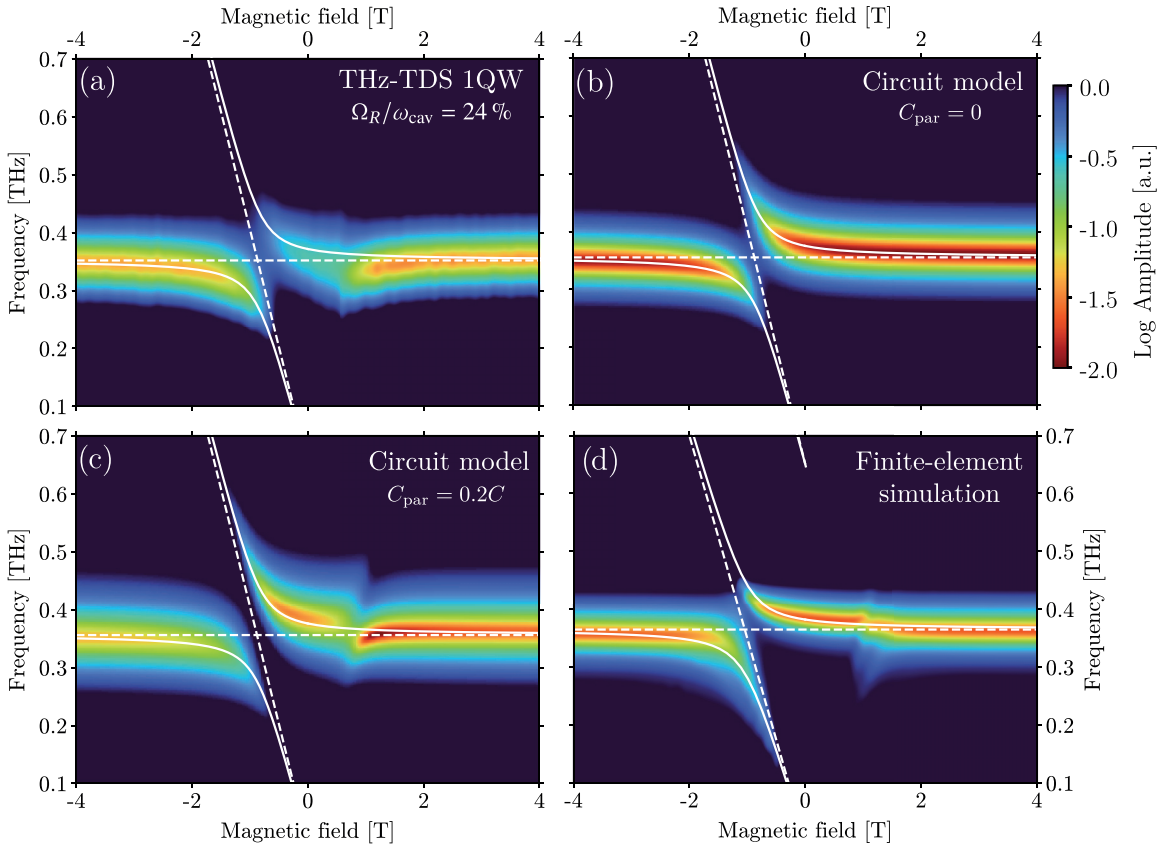

FIG. 3. (a) THz-TDS measurement for a single quantum well sample as a function of perpendicular magnetic field together with a fit of the Hopfield model with circular polarization [19] using the LP mode. (b) and (c) show the simulated transmission of the circuit model with and without parasitic capacitive coupling between the orthogonal antennas, respectively. (d) Finite-element simulation of the transmission of the cavity, modeling the 2DEG as a gyrotropic material.

the degree of chirality of the cavity. In a next step the direct effect of the electromagnetic vacuum field on the 2DEG can be investigated by means of magnetotransport measurements in a van der Pauw configuration [35], taking advantage of the symmetry of the chiral cavity.

By further reducing the gap size this system also offers the possibility of exploring the few-electron regime beyond the dilute regime of few excitations in which the Hopfield model is valid [36]. Additionally, it can be used with a variety of 2D materials such as graphene, instead of the GaAs/AlGaAs quantum wells used here.

Since emphasis was placed on conceptual simplicity in the design, other geometries that would suffer less from parasitic capacitive coupling between the modes can be explored, for example, ones where the gap is surrounded by three antennas instead of four.

The effect of the circularly polarized ground state of the cavity on other systems could be studied by bringing them into close physical proximity with its capacitor gap. However, one aspect that has not been fully explored in this Letter are the effects of using an array of nanoantennas compared to just a single cross, in particular how the chiral character of the electric field inside one gap is modified by its neighbors since they are coupled via their mutual inductance. If the array can be utilized as a coupled cavity system to impose a chiral electric field distribution onto a gap without 2DEG, this could enable studying the effect of a chiral electromagnetic ground state on other systems, with the caveat of the presence of the external magnetic field.

Acknowledgment. The authors acknowledge the FIRST-Lab cleanroom where the majority of the fabrication process took place, S. Rajabali for her work on the nanoantennas that served as a starting point for the design of the chiral metamaterial cavities and her ideas on mitigating the issue of polaritonic nonlocality, A. Rubio for discussions, and the funding and support provided by the Swiss National Science Foundation (Project No. 200020-207795) through the National Centre of Competence in Research Quantum Science and Technology (NCCR QSIT) and by the Alexander von Humboldt Stiftung through the Humboldt Research Award awarded to J.F.

[1] B. Keimer and J. Moore, The physics of quantum materials, Nat. Phys. **13**, 1045 (2017).

[2] K. von Klitzing, The quantized Hall effect, Rev. Mod. Phys. **58**, 519 (1986).

[3] T. Oka and H. Aoki, Photovoltaic Hall effect in graphene, Phys. Rev. B **79**, 081406(R) (2009).

[4] N. H. Lindner, G. Refael, and V. Galitski, Floquet topological insulator in semiconductor quantum wells, Nat. Phys. **7**, 490 (2011).

[5] Y. Wang, H. Steinberg, P. Jarillo-Herrero, and N. Gedik, Observation of Floquet-Bloch states on the surface of a topological insulator, Science **342**, 453 (2013).

[6] J. W. McIver, B. Schulte, F.-U. Stein, T. Matsuyama, G. Jotzu, G. Meier, and A. Cavalleri, Light-induced anomalous Hall effect in graphene, Nat. Phys. **16**, 38 (2020).

[7] J. C. Owens, M. G. Panetta, B. Saxberg, G. Roberts, S. Chakram, R. Ma, A. Vrajitoarea, J. Simon, and D. I. Schuster, Chiral cavity quantum electrodynamics, Nat. Phys. **18**, 1048 (2022).

[8] C. Owens, A. LaChapelle, B. Saxberg, B. M. Anderson, R. Ma, J. Simon, and D. I. Schuster, Quarter-flux Hofstadter lattice in a qubit-compatible microwave cavity array, Phys. Rev. A **97**, 013818 (2018).

[9] Z. Wang, Y. Chong, J. D. Joannopoulos, and M. Soljačić, Observation of unidirectional backscattering-immune topological electromagnetic states, Nature (London) **461**, 772 (2009).

[10] X. Wang, E. Ronca, and M. A. Sentef, Cavity quantum electrodynamical Chern insulator: Towards light-induced quantized anomalous Hall effect in graphene, Phys. Rev. B **99**, 235156 (2019).

[11] C. Ciuti, G. Bastard, and I. Carusotto, Quantum vacuum properties of the intersubband cavity polariton field, Phys. Rev. B **72**, 115303 (2005).

[12] H. Hübener, U. De Giovannini, C. Schäfer, J. Andberger, M. Ruggenthaler, J. Faist, and A. Rubio, Engineering quantum materials with chiral optical cavities, Nat. Mater. **20**, 438 (2021).

[13] D. Hagenmüller, S. De Liberato, and C. Ciuti, Ultrastrong coupling between a cavity resonator and the cyclotron transition of a two-dimensional electron gas in the case of an integer filling factor, Phys. Rev. B **81**, 235303 (2010).

[14] G. Scalari, C. Maissen, D. Turčinková, D. Hagenmüller, S. De Liberato, C. Ciuti, C. Reichl, D. Schuh, W. Wegscheider, M. Beck, and J. Faist, Ultrastrong coupling of the cyclotron transition of a 2D electron gas to a THz metamaterial, Science **335**, 1323 (2012).

[15] G. L. Paravicini-Bagliani, F. Appugliese, E. Richter, F. Valmorra, J. Keller, M. Beck, N. Bartolo, C. Rössler, T. Ihn, K. Ensslin *et al.*, Magneto-transport controlled by Landau polariton states, Nat. Phys. **15**, 186 (2019).

[16] F. Appugliese, J. Enkner, G. L. Paravicini-Bagliani, M. Beck, C. Reichl, W. Wegscheider, G. Scalari, C. Ciuti, and J. Faist, Breakdown of topological protection by cavity vacuum fields in the integer quantum Hall effect, Science **375**, 1030 (2022).

[17] E. Mavrona, S. Rajabali, F. Appugliese, J. Andberger, M. Beck, G. Scalari, and J. Faist, THz ultrastrong coupling in an engineered Fabry–Perot cavity, ACS Photonics **8**, 2692 (2021).

[18] J. J. Hopfield, Theory of the contribution of excitons to the complex dielectric constant of crystals, Phys. Rev. **112**, 1555 (1958).

[19] X. Li, M. Bamba, Q. Zhang, S. Fallahi, G. C. Gardner, W. Gao, M. Lou, K. Yoshioka, M. J. Manfra, and J. Kono, Vacuum Bloch–Siegert shift in Landau polaritons with ultra-high cooperativity, Nat. Photon. **12**, 324 (2018).

[20] F. De Zela, E. Solano, and A. Gago, Micromaser without the rotating-wave approximation: The Bloch-Siegert shift and related effects, Opt. Commun. **142**, 106 (1997).

[21] See Supplemental Material at http://link.aps.org/supplemental/10.1103/PhysRevB.109.L161302 for the quantum mechanical theory used to fit the coupling strength, the circuit theory model accounting for the effect of broken time-reversal symmetry and with and without parasitic capacitive interaction between the orthogonal antennas outside the 2DEG, finite-element simulations of the coupled system, and the heterostructures and fabrication process and transmission THz-TDS measurement using linear polarization.

[22] S. Messelot, S. Coeymans, J. Tignon, S. Dhillon, and J. Mangeney, High Q and sub-wavelength THz electric field confinement in ultrastrongly coupled THz resonators, Photon. Res. **11**, 1203 (2023).

[23] C. Feuillet-Palma, Y. Todorov, A. Vasanelli, and C. Sirtori, Strong near field enhancement in THz nano-antenna arrays, Sci. Rep. **3**, 1361 (2013).

[24] L. V. Poulikakos, P. Gutsche, K. M. McPeak, S. Burger, J. Niegemann, C. Hafner, and D. J. Norris, Optical chirality flux as a useful far-field probe of chiral near fields, ACS Photonics **3**, 1619 (2016).

[25] G. L. Paravicini-Bagliani, G. Scalari, F. Valmorra, J. Keller, C. Maissen, M. Beck, and J. Faist, Gate and magnetic field tunable ultrastrong coupling between a magnetoplasmon and the optical mode of an LC cavity, Phys. Rev. B **95**, 205304 (2017).

[26] E. Cortese, I. Carusotto, R. Colombelli, and S. D. Liberato, Strong coupling of ionizing transitions, Optica **6**, 354 (2019).

[27] S. Rajabali, E. Cortese, M. Beck, S. De Liberato, J. Faist, and G. Scalari, Polaritonic nonlocality in light–matter interaction, Nat. Photon. **15**, 690 (2021).

[28] S. Rajabali, J. Enkner, E. Cortese, M. Beck, S. D. Liberato, J. Faist, and G. Scalari, Engineered planar plasmonic reflector for polaritonic mode confinement, Opt. Mater. Express **13**, 2944 (2023).

[29] D. Grischkowsky, S. Keiding, M. van Exter, and C. Fattinger, Far-infrared time-domain spectroscopy with terahertz beams of dielectrics and semiconductors, J. Opt. Soc. Am. B **7**, 2006 (1990).

[30] X. Xia and J. J. Quinn, Edge magnetoplasmons of two-dimensional electron-gas systems, Phys. Rev. B **50**, 11187 (1994).

[31] T. Ihn, *Semiconductor Nanostructures: Quantum States and Electronic Transport* (Oxford University Press, Oxford, UK, 2009).

[32] C. Balanis, *Antenna Theory: Analysis and Design* (Wiley, New York, 1996).

[33] J. Kraus, *Antennas*, Electrical Engineering Series (McGraw-Hill, New York, 1950).

[34] J. A. Curtis, T. Tokumoto, A. T. Hatke, J. G. Cherian, J. L. Reno, S. A. McGill, D. Karaiskaj, and D. J. Hilton, Cyclotron decay

time of a two-dimensional electron gas from 0.4 to 100 K, Phys. Rev. B **93**, 155437 (2016).

[35] L. J. van der Pauw, A method of measuring specific resistivity and Hall effect of discs of arbitrary shape, Philips Res. Rep **13**, 1 (1958).

[36] J. Keller, G. Scalari, S. Cibella, C. Maissen, F. Appugliese, E. Giovine, R. Leoni, M. Beck, and J. Faist, Few-electron ultrastrong light-matter coupling at 300 GHz with nanogap hybrid LC microcavities, Nano Lett. **17**, 7410 (2017).